galaxies

MDPI

Conference Report

Constraints on the Formation of M31's Stellar Halo from the SPLASH Survey

Karoline Gilbert [1,2]

[1] Space Telescope Science Institute, 3700 San Martin Dr, Baltimore, MD 21218, USA; kgilbert@stsci.edu; Tel.: +1-410-338-2475

[2] Department of Physics & Astronomy, Johns Hopkins University, Baltimore, MD 21218, USA

Academic Editors: Duncan A. Forbes and Ericson D. Lopez
Received: 16 August 2017; Accepted: 13 September 2017; Published: 30 September 2017

Abstract: The SPLASH (Spectroscopic and Photometric Landscape of Andromeda's Stellar Halo) Survey has observed fields throughout M31's stellar halo, dwarf satellites, and stellar disk. The observations and derived measurements have either been compared to predictions from simulations of stellar halo formation or modeled directly in order to derive inferences about the formation and evolution of M31's stellar halo. We summarize some of the major results from the SPLASH survey and the resulting implications for our understanding of the build-up of M31's stellar halo.

Keywords: galaxies: evolution; galaxies: halos; galaxies: individual (M31)

---

1. Introduction

Observations of stellar halos provide the potential to decipher both the early and recent merger histories of nearby galaxies (Figure 1). Recent accretion events are visible as strong enhancements in stellar density, and typically as kinematically cold features in stellar velocity distributions. These features can be modeled in detail to determine the properties of the progenitor system and its orbit (e.g., [1]). Simulations of stellar halo formation in a cosmological context make predictions for the global properties (e.g., stellar density profiles, metallicity gradients, and fraction of stars formed in situ and accreted) of stellar halos for hosts spanning a range of masses and merger histories (e.g., [2–5]). Suites of simulated stellar halos enable comparisons of the observed global properties of stellar halos to simulations to make inferences about the early accretion history of the halos.

The proximity of the Andromeda galaxy (M31) provides a unique opportunity to study the global properties of a stellar halo in great detail. The ability to make measurements of individually resolved stars is powerful, enabling measurements of the stellar density to very low surface brightness, stellar line of sight velocities, chemical abundances, and star formation histories. This has led to a significant investment of time spent observing M31, including by the SPLASH (Spectroscopic and Photometric Landscape of Andromeda's Stellar Halo), PAndAS (Pan-Andromeda Archaeological Survey; e.g., [6,7]), and PHAT (Panchromatic Hubble Andromeda Treasury; [8]) teams. Here we summarize the contributions to understanding the formation and evolution of M31's stellar halo made by the SPLASH survey.

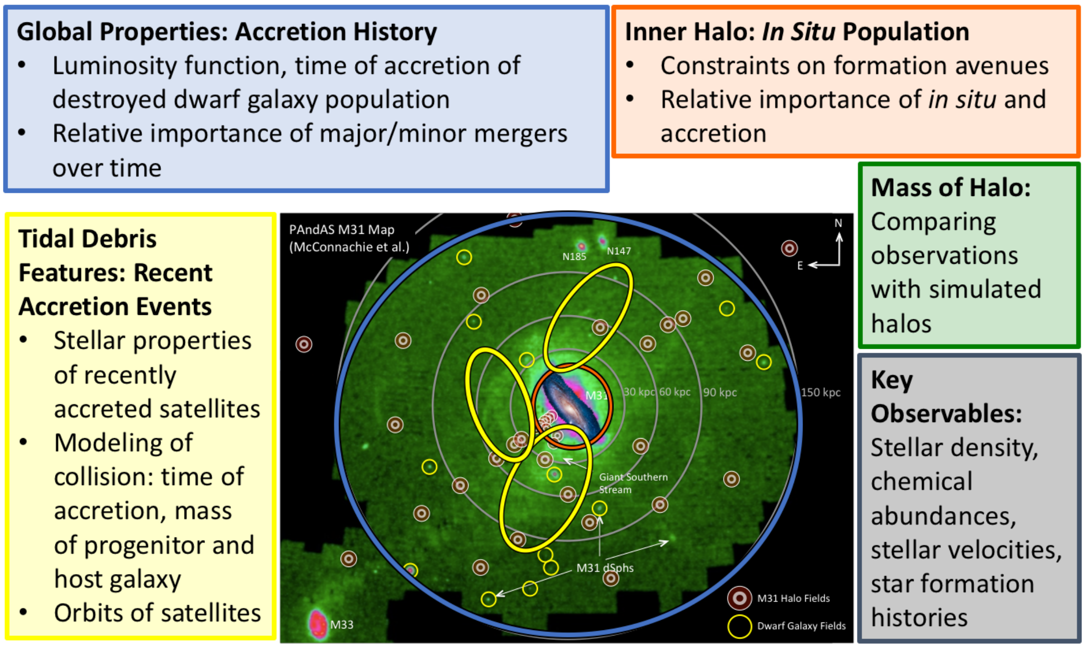

Figure 1. A summary of what can be learned from observations of stellar halos. The underlying figure (Figure 2 of [9]) portrays the stellar surface density of M31's stellar halo, and was generated from resolved star counts derived from images obtained with the MegaCam instrument on the Canada-France-Hawaii Telescope by the PAndAS survey [6].

2. The SPLASH Survey

The SPLASH collaboration has obtained photometry and spectroscopy of fields throughout M31's stellar halo and disk.

Photometry was primarily obtained with the Mosaic camera on the Kitt Peak 4 m Mayall Telescope, imaging 78 fields in the broad-band M and T_2 filters, and the narrow-band DDO51 filter (PIs S. Majewski and R. Beaton). The DDO51 filter overlaps the surface-gravity-sensitive Mg b and MgH stellar ab-sorption features, which are strong in dwarf stars but weak in red giant branch (RGB) stars. This filter combination allows for the photometric pre-selection of stars likely to be M31 red giant branch stars (e.g., [10]), greatly increasing our spectroscopic efficiency over a large region of M31's stellar halo. We have also utilized broad-band photometry obtained with SuprimeCam on Subaru, and Hubble Space Telescope imaging of M31's disk.

Spectroscopy of individual stars was obtained with the DEIMOS spectrograph on the Keck II 10 m telescope, primarily at $R \sim 6000$. The SPLASH collaboration has obtained more than 20,000 M31 stellar spectra in $\sim$170 spectroscopic masks targeting Andromeda's disk, dwarf galaxies, and halo, in fields ranging from 2 to 230 kpc in projected distance from Andromeda's center (Figure 2).

The SPLASH dataset has led to the discovery and characterization of Andromeda's extended metal-poor stellar halo [11–14]. In addition to the studies discussed below (global properties, identification and characterization of tidal debris features), it has also been used to study Andromeda's dwarf satellites [15–21] and to characterize M31's stellar disk [22].

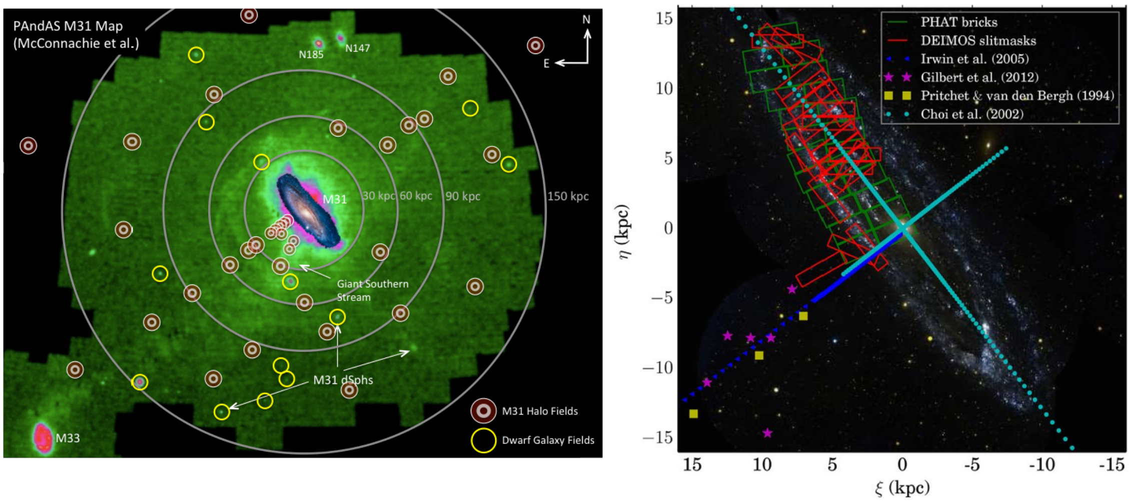

Figure 2. The locations of M31 halo and disk spectroscopic fields in the SPLASH survey. (**Left**) Fields targeting M31's halo, tidal debris features, and dwarf galaxies, superimposed on a stellar density map created from the Pan-Andromeda Archaeological Survey (PAndAS) observations [23] (Figure 2 of Gilbert et al. [9]). (**Right**) Fields targeting M31's disk; many of these spectroscopic masks were designed using photometry from the Hubble Space Telescope Multi Cycle Treasury Program PHAT (Figure 3 of Dorman et al. [24]).

3. The Properties of M31's Halo Measured by SPLASH

Below, we briefly summarize a selection of measurements made with the SPLASH dataset and their implications for the formation and evolution of Andromeda and its stellar halo.

In each study, spectroscopic and photometric measurements were used to identify secure samples of M31 RGB stars, enabling us to remove Milky Way dwarf star contaminants (e.g., [12]). The stellar velocity distributions in each field were used to identify stars that were likely to be associated with kinematically cold tidal debris features (e.g., [25–27]).

3.1. Global Properties of Andromeda's Stellar Halo

3.1.1. Surface Brightness and Metallicity Profiles

SPLASH observations in 38 halo fields, spanning all quadrants of the halo and ranging from 9 to 230 kpc in projected distance from the center of M31 (Figure 2), have been used to measure the surface brightness and metallicity profiles of M31's stellar halo.

The surface brightness profile of Andromeda's stellar halo is consistent with a single power-law with a power law index of -2.2 ± 0.2, extending to a projected distance of more than 175 kpc from M31's center (Figure 3; [27]). This is true regardless of whether tidal debris features are included in the profile, although the inclusion of tidal debris features does affect the normalization and index of the power-law fit. A similar surface brightness profile was found using the PAndAS star count data [7], and an extension of a power-law profile into the inner regions of M31 (to 3 kpc in projected distance from M31's center) was observed in blue horizontal branch stars with PHAT data [28,29].

There is no sign of a downward break in the surface brightness profile, out to $\sim$2/3 of the estimated virial radius ($\sim$260 kpc; [30]). This was found to be atypical of simulated stellar halos, most of which do display a break in the surface brightness profile well within the range of projected radii probed by the SPLASH dataset. In the Bullock and Johnston [2] simulated halos, the only halo without a downward break in the stellar density profile is the one with many recent low-mass accretions. Future observations of the outer halo of M31—including measurements of the [Fe/H] and [α/Fe] abundances [31,32]—could confirm whether the stars in the outer halo are consistent with such a scenario: the mean [Fe/H] of a dwarf galaxy is strongly correlated with its luminosity (e.g., [33]), while the [α/Fe] abundance is sensitive to the timescale over which stars formed (e.g., [34]). Together, the [Fe/H] and [α/Fe] abundances of halo stars can thus be used to infer the luminosity and time since accretion of the dwarf satellite progenitors (e.g., [1,2,35]).

The SPLASH data also reveal that Andromeda's stellar halo has a significant gradient in metallicity out to projected distances of $\sim$100 kpc [36], with a total decrease of $\sim$1 dex. A significant gradient is observed whether or not tidal debris features are included in the measurement. The [Fe/H] measurements shown in Figure 3 are for a spectroscopically selected set of M31 RGB stars, but are based on photometry. Spectroscopic estimates of [Fe/H] for a subset of the highest S/N spectra, based on the equivalent width of the calcium triplet, result in a consistent gradient of metallicity with radius. A decrease in metallicity with radius was also observed in the PAndAS data [7].

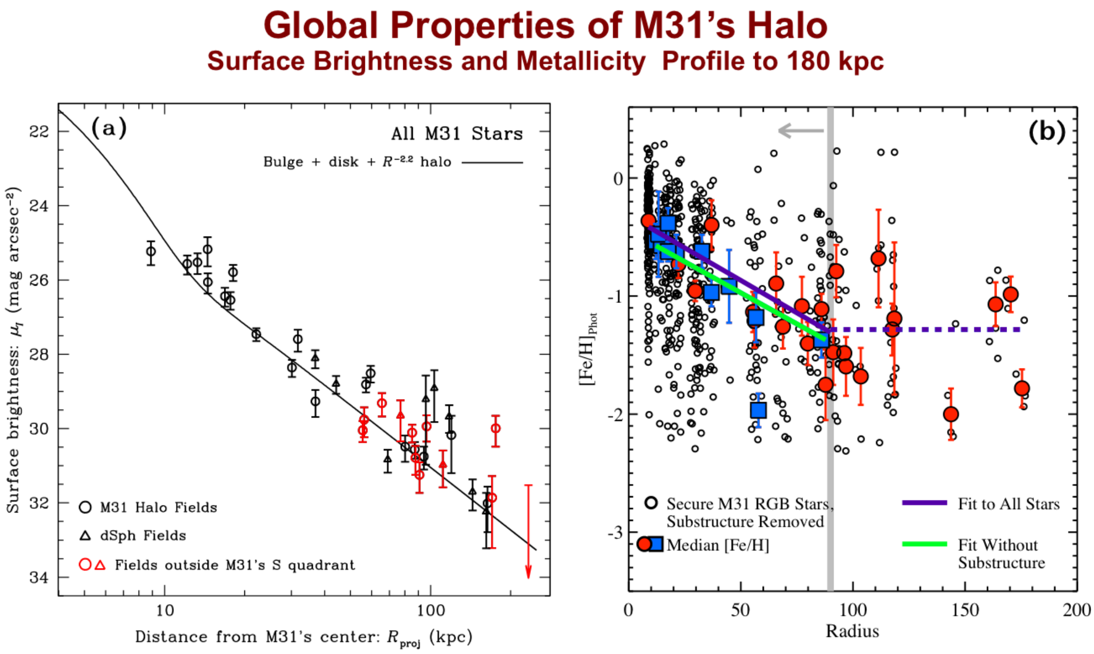

Figure 3. (**a**) The surface brightness profile of M31's stellar halo from the SPLASH survey (Figure 6 of Gilbert et al. [27]). The number of spectroscopically confirmed M31 RGB and Milky Way (MW) dwarf stars is used to determine the surface brightness in each SPLASH spectroscopic field. The surface brightness profile of halo stars after tidal debris features have been removed follows an $r^{-2.2}$ power law to large distances from M31's center. (**b**) Metallicity profile of M31's stellar halo from the SPLASH survey (Figure 10 of Gilbert et al. [36]). Metallicity estimates are based on comparing the position of the star in the color magnitude diagram to a grid of isochrones at the distance of M31. All spectroscopically confirmed M31 RGB stars that are not associated with tidal debris features are shown as small, open black points; the median metallicity and estimated uncertainty in the median value are shown as large, solid red circles (fields without tidal debris features) and blue squares (fields with tidal debris features). No tidal debris features are identified in fields greater than 90 kpc from the center of M31, in which the samples of M31 stars are small. M31's halo shows a significant gradient with metallicity to at least 100 kpc. The solid lines show fits to the median metallicity in fields out to 90 kpc, while the dashed line shows the median metallicity of stars in fields at projected distances >90 kpc from M31's center.

Based on comparisons with simulations of stellar halo formation [3,5], the observed large-scale metallicity gradient extending over $\sim$100 kpc may indicate that the majority of the stars in the halo were contributed by one to a few early and relatively massive accretion events (see discussion in [36]). This hypothesis can be tested with future observations of [Fe/H] and [α/Fe] abundances of stars in M31's halo.

3.1.2. Stellar Velocity Dispersion

Gilbert et al. [9] have modeled the velocity distribution of stars in M31's stellar halo, using a set of 50 spectroscopic fields. We used Markov Chain Monte Carlo techniques to sample the parameter space of a Gaussian mixture model that includes the M31 halo, all known M31 tidal debris features in our fields, as well as three components for the MW contamination (disk, thick disk, and halo). The model also includes the probability that a star is an M31 RGB star or a MW dwarf star as a prior. This procedure was performed in a series of radial bins, in order to trace the change in velocity dispersion of M31's stellar halo with projected distance from M31's center.

M31's stellar halo appears to have a fairly flat velocity dispersion profile with radius (Figure 4). The velocity dispersion of M31's stellar halo was found to be significantly flatter than that observed in M31's globular cluster system by the PAndAS team [37]. It should be noted that in addition to probing two distinct halo tracers, these studies have two significant differences, each of which could affect the measured slope of the power-law: [37] included rotation in the model, but did not account for tidal debris features, while [9] fit for tidal debris features, but (as shown here) did not include rotation in the model.

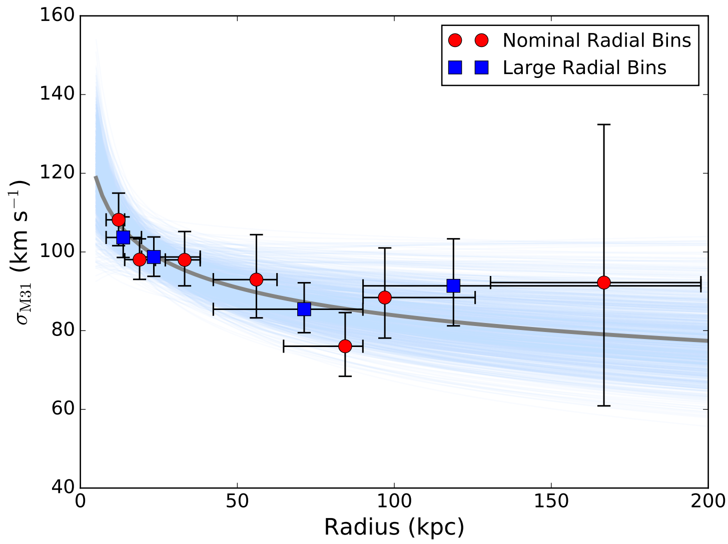

Figure 4. The stellar velocity dispersion of M31's halo as a function of projected distance from M31's center (Figure 10 of Gilbert et al. [9]). Points, placed at the median radius of all stars in the bin (with error bars denoting the full range of radii), show the 50th percentile of the marginalized one-dimensional posterior probability distribution for the velocity dispersion, with the error bar denoting the 16th to 84th percentile. The light blue curves show a subset of power-law fits to random draws from the posteriors; the dark gray curve shows a power-law defined by the 50th percentile values for the normalization and slope distributions. The velocity dispersion of stars in M31's halo remains relatively flat, with only a weak gradient, out to large radii.

This analysis provides a third global profile for comparing to simulations of stellar halo formation. Furthermore, since all known M31 tidal debris features in the spectroscopic fields were included in the model, we now have more precise constraints on the kinematical properties of these features, along with a significantly improved understanding of the uncertainties on the relevant parameters.

In the future, this analysis can be leveraged to provide a constraint on M31's total mass, using a separate set of halo tracers than the globular cluster and dwarf satellite systems. This can be done either through the use of the profile itself in conjunction with mass estimators such as that of Wolf et al. [38], or by using the velocities of the stars themselves along with tracer mass estimator techniques (e.g., [37,39]).

3.2. Tidal Debris Features

The velocity distributions of spectroscopically confirmed M31 stars in individual fields have been analyzed to identify and characterize tidal debris features, including measurements along the giant southern stream (GSS)—the most prominent tidal stream in M31's stellar halo [25–27,35,40,41].

These measurements also include the discovery of the continuation of the GSS [25,42,43], which forms a shell system in the inner regions of M31's halo. In conjunction with the giant southern stream itself, observations of the shells created by the progenitor of the GSS provide sensitive constraints for modeling the interaction of the progenitor with M31, as shown in Figure 5. Modeling of these features yields detailed inferences for the properties of the progenitor and its orbit (a dwarf galaxy with stellar mass comparable to that of the Large Magellanic Cloud ($\log M = 9.5 \pm 0.1$), with the disruptive pericentric passage occurring 760 ± 50 Myr ago), as well as constraints on the total mass of M31 ($M_{200} \sim 2 \times 10^{12}\, M_\odot$) [44].

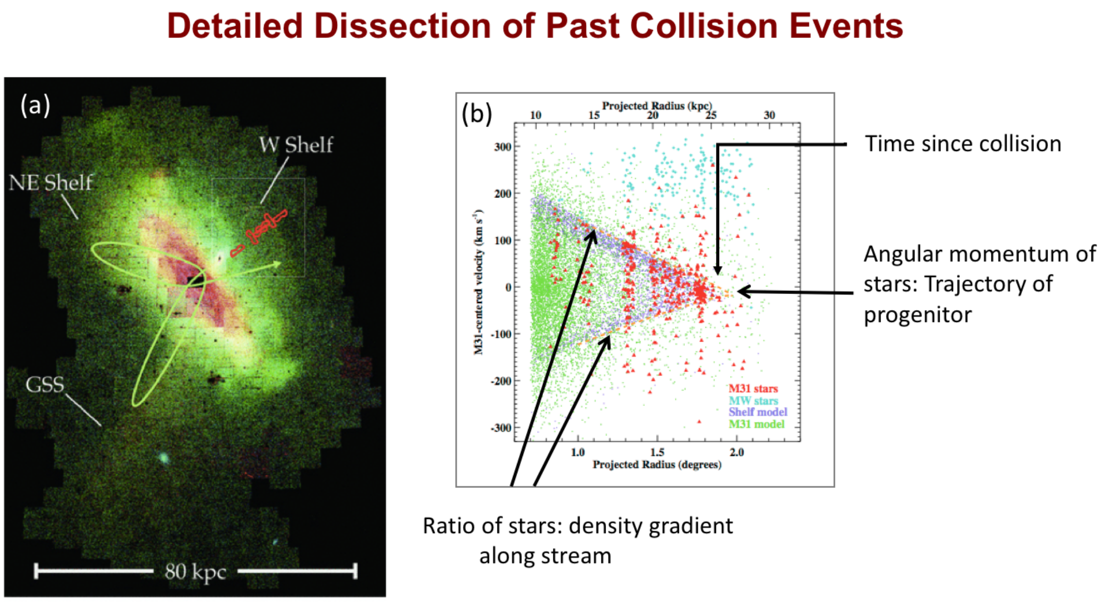

Figure 5. Shell systems, such as that created by the progenitor of the giant southern stream (GSS), provide exquisite observational constraints for modeling the orbit and properties of the dwarf satellite progenitor. Since confirmed as a shell system through the prediction and discovery of the southeast shelf [25,42], observations of the western shelf (shown here), in conjunction with previous observations of the GSS and southeast shelf, were used to determine the mass and disruption time of the progenitor, and to constrain the mass of M31 [44]. (**a**) Star count map of M31's inner halo, derived from the INT survey of M31 (image created by M. Irwin [45]), with the location of the SPLASH spectroscopic slitmasks covering the western shelf region overlaid in red (Figure 1 of Fardal et al. [43]). The green curve shows the progenitor's path in the model of Fardal et al. [43]. (**b**) M31-centric velocity ersus projected distance from M31's center for observed M31 stars (large red points) and simulated particles (Figure 8 of Fardal et al. [43]). A quantitative comparison of data with the simulations can constrain the orbit and properties of the progenitor system: the ratio of stars in the upper and lower caustic of the shell feature constrains the density gradient along the stream, while the location of the tip of the feature in projected distance and velocity is sensitive to the time since the disruptive pericentric passage and the angular momentum of the stars, respectively.

3.3. Andromeda's Inner Halo

Dorman et al. [24] modeled the relative contributions of M31's bulge, disk, and halo with radius, using a combination of stellar kinematics in M31's disk from SPLASH (Figure 2), the stellar luminosity function from resolved HST imaging (PHAT; [8] also shown in Figure 2), and unresolved surface photometry. The best fitting models had a disk fraction that was in significant tension with the fraction of stars with disk-like (dynamically cold) kinematics as measured from the velocity distribution of the stars. The disk fraction favored by analyzing all datasets in conjunction is $5.2 \pm 2.1\%$ higher than the fraction of stars with disk-like kinematics. Earlier work by Dorman et al. [46] also measured significant rotation for stars with halo-like kinematics in the inner halo of M31.

This is the first observational evidence for a population of halo stars that formed in the disk and were subsequently dynamically heated into halo-like orbits. While cosmological hydrodynamical simulations of stellar halo formation predict this as a mechanism for forming a portion of the inner regions of stellar halos (e.g., [47–49]), simulations differ in their predictions of the relative importance of this mechanism in terms of the fraction of stellar halo stars originally formed in a disk (see Section 6.1 of Dorman et al. [46] for a detailed discussion). Further observations, such as measurements of the [Fe/H] and [α/Fe] abundances of stars with halo-like kinematics, could lead to stronger constraints on the distribution of stars heated from M31's disk, since the different star formation histories of disk stars and halo stars will result in significant differences in the distribution of [α/Fe] as a function of [Fe/H].

4. Conclusions

The Andromeda system provides a unique testbed for furthering our physical understanding of galaxy formation and evolution. By observing individual stars throughout M31's stellar halo, we can probe the early accretion history of M31, constrain the fraction of stars in the inner halo that were once part of M31's disk, model the orbits and properties of recently disrupted dwarf satellites, and constrain the total mass of M31. Figure 6 summarizes the inferences that have been made regarding the formation of M31's stellar halo through the use of the SPLASH dataset. Further observations—in particular chemical abundance measurements of individual stars—hold much promise for furthering our understanding of the formation of M31's stellar halo.

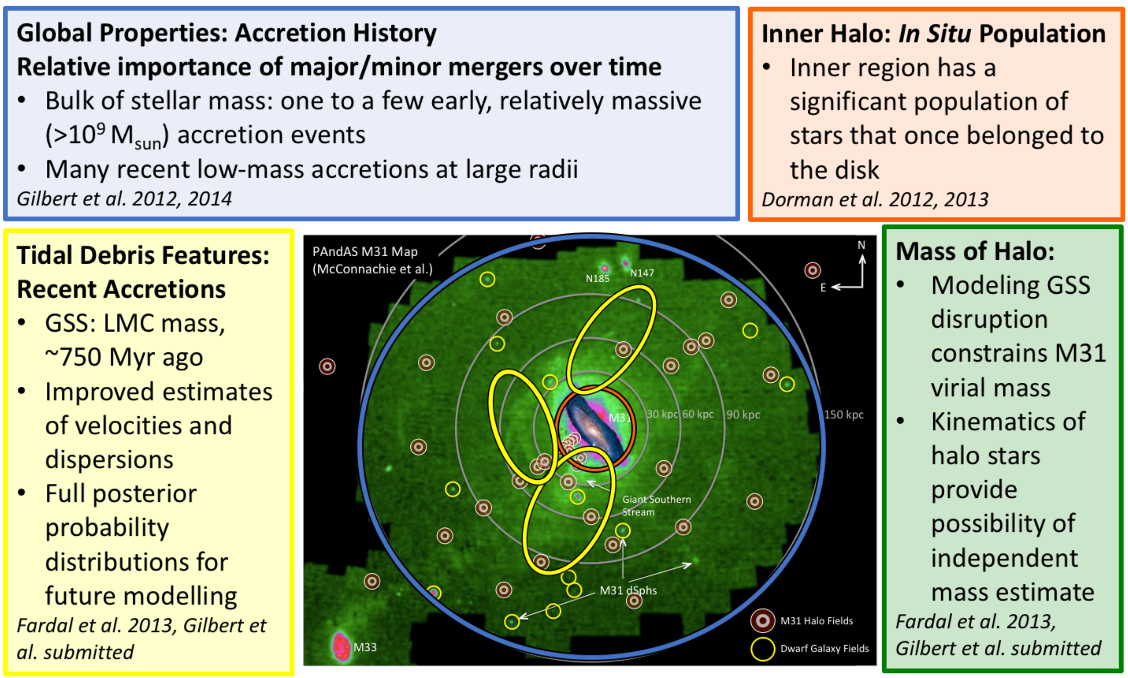

Figure 6. A summary of the major inferences that can be made about the formation of M31's stellar halo from measurements made using the SPLASH dataset. The underlying figure is the same as in Figure 1.

Acknowledgments: I thank the SPLASH team for their contributions to the work summarized here.

Conflicts of Interest: The author declares no conflict of interest.

Abbreviations

The following abbreviations are used in this manuscript:

M31	Andromeda
MW	Milky Way
PAndAS	Pan-Andromeda Archaeological Survey
PHAT	Panchromatic Hubble Andromeda Treasury
RGB	red giant branch
SPLASH	Spectroscopic and Photometric Landscape of Andromeda's Stellar Halo

References

1. Johnston, K.V.; Bullock, J.S.; Sharma, S.; Font, A.; Robertson, B.E.; Leitner, S.N. Tracing Galaxy Formation with Stellar Halos. II. Relating Substructure in Phase and Abundance Space to Accretion Histories. *Astrophys. J.* **2008**, *689*, 936–957.
2. Bullock, J.S.; Johnston, K.V. Tracing Galaxy Formation with Stellar Halos. I. Methods. *Astrophys. J.* **2005**, *635*, 931–949.
3. Cooper, A.P.; Cole, S.; Frenk, C.S.; White, S.D.M.; Helly, J.; Benson, A.J.; De Lucia, G.; Helmi, A.; Jenkins, A.; Navarro, J.F.; et al. Galactic stellar haloes in the CDM model. *Mon. Not. R. Astron. Soc.* **2010**, *406*, 744–766.
4. Font, A.S.; McCarthy, I.G.; Crain, R.A.; Theuns, T.; Schaye, J.; Wiersma, R.P.C.; Vecchia, C.D. Cosmological simulations of the formation of the stellar haloes around disc galaxies. *Mon. Not. R. Astron. Soc.* **2011**, *416*, 2802–2820.
5. Tissera, P.B.; Beers, T.C.; Carollo, D.; Scannapieco, C. Stellar haloes in Milky Way mass galaxies: From the inner to the outer haloes. *Mon. Not. R. Astron. Soc.* **2014**, *439*, 3128–3138.
6. McConnachie, A.W.; Irwin, M.J.; Ibata, R.A.; Dubinski, J.; Widrow, L.M.; Martin, N.F.; Côté, P.; Dotter, A.L.; Navarro, J.F.; Ferguson, A.M.N.; et al. The remnants of galaxy formation from a panoramic survey of the region around M31. *Nature* **2009**, *461*, 66–69.
7. Ibata, R.A.; Lewis, G.F.; McConnachie, A.W.; Martin, N.F.; Irwin, M.J.; Ferguson, A.M.N.; Babul, A.; Bernard, E.J.; Chapman, S.C.; Collins, M.; et al. The Large-scale Structure of the Halo of the Andromeda Galaxy. I. Global Stellar Density, Morphology and Metallicity Properties. *Astrophys. J.* **2014**, *780*, 128.
8. Dalcanton, J.J.; Williams, B.F.; Lang, D.; Lauer, T.R.; Kalirai, J.S.; Seth, A.C.; Dolphin, A.; Rosenfield, P.; Weisz, D.R.; Bell, E.F.; et al. The Panchromatic Hubble Andromeda Treasury. *Astrophys. J. Suppl.* **2012**, *200*, 18.
9. Gilbert, K.M.; Tollerud, E.; Beaton, R.L.; Guhathakurta, P.; Bullock, J.S.; Chiba, M.; Kalirai, J.S.; Kirby, E.N.; Majewski, S.R.; Tanaka, M. Global Properties of M31's Stellar Halo From the SPLASH Survey: III. Measuring the Stellar Velocity Dispersion Profile. *Astrophys. J.* **2017**, submitted.
10. Palma, C.; Majewski, S.R.; Siegel, M.H.; Patterson, R.J.; Ostheimer, J.C.; Link, R. Exploring Halo Substructure with Giant Stars. IV. The Extended Structure of the Ursa Minor Dwarf Spheroidal Galaxy. *Astron. J.* **2003**, *125*, 1352–1372.
11. Guhathakurta, P.; Ostheimer, J.C.; Gilbert, K.M.; Rich, R.M.; Majewski, S.R.; Kalirai, J.S.; Reitzel, D.B.; Patterson, R.J. Discovery of an extended halo of metal-poor stars in the Andromeda spiral galaxy. *ArXiv* **2005**, arXiv:astro-ph/0502366.
12. Gilbert, K.M.; Guhathakurta, P.; Kalirai, J.S.; Rich, R.M.; Majewski, S.R.; Ostheimer, J.C.; Reitzel, D.B.; Cenarro, A.J.; Cooper, M.C.; Luine, C.; et al. A New Method for Isolating M31 Red Giant Stars: The Discovery of Stars out to a Radial Distance of 165 kpc. *Astrophys. J.* **2006**, *652*, 1188–1212.
13. Kalirai, J.S.; Gilbert, K.M.; Guhathakurta, P.; Majewski, S.R.; Ostheimer, J.C.; Rich, R.M.; Cooper, M.C.; Reitzel, D.B.; Patterson, R.J. The Metal-poor Halo of the Andromeda Spiral Galaxy (M31). *Astrophys. J.* **2006**, *648*, 389–404.
14. Courteau, S.; Widrow, L.M.; McDonald, M.; Guhathakurta, P.; Gilbert, K.M.; Zhu, Y.; Beaton, R.L.; Majewski, S.R. The Luminosity Profile and Structural Parameters of the Andromeda Galaxy. *Astrophys. J.* **2011**, *739*, 20–36.

15. Majewski, S.R.; Beaton, R.L.; Patterson, R.J.; Kalirai, J.S.; Geha, M.C.; Muñoz, R.R.; Seigar, M.S.; Guhathakurta, P.; Gilbert, K.M.; Rich, R.M.; et al. Discovery of Andromeda XIV: A Dwarf Spheroidal Dynamical Rogue in the Local Group? *Astrophys. J. Lett.* **2007**, *670*, L9–L12.
16. Kalirai, J.S.; Zucker, D.B.; Guhathakurta, P.; Geha, M.; Kniazev, A.Y.; Martínez-Delgado, D.; Bell, E.F.; Grebel, E.K.; Gilbert, K.M. The SPLASH Survey: A Spectroscopic Analysis of the Metal-Poor, Low-Luminosity M31 dSph Satellite Andromeda X. *Astrophys. J.* **2009**, *705*, 1043–1055.
17. Howley, K.M.; Geha, M.; Guhathakurta, P.; Montgomery, R.M.; Laughlin, G.; Johnston, K.V. Darwin Tames an Andromeda Dwarf: Unraveling the Orbit of NGC 205 Using a Genetic Algorithm. *Astrophys. J.* **2008**, *683*, 722–749.
18. Kalirai, J.S.; Beaton, R.L.; Geha, M.C.; Gilbert, K.M.; Guhathakurta, P.; Kirby, E.N.; Majewski, S.R.; Ostheimer, J.C.; Patterson, R.J.; Wolf, J. The SPLASH Survey: Internal Kinematics, Chemical Abundances, and Masses of the Andromeda I, II, III, VII, X, and XIV Dwarf Spheroidal Galaxies. *Astrophys. J.* **2010**, *711*, 671–692.
19. Tollerud, E.J.; Beaton, R.L.; Geha, M.C.; Bullock, J.S.; Guhathakurta, P.; Kalirai, J.S.; Majewski, S.R.; Kirby, E.N.; Gilbert, K.M.; Yniguez, B.; et al. The SPLASH Survey: Spectroscopy of 15 M31 Dwarf Spheroidal Satellite Galaxies. *Astrophys. J.* **2012**, *752*, 45.
20. Ho, N.; Geha, M.; Munoz, R.R.; Guhathakurta, P.; Kalirai, J.; Gilbert, K.M.; Tollerud, E.; Bullock, J.; Beaton, R.L.; Majewski, S.R. Stellar Kinematics of the Andromeda II Dwarf Spheroidal Galaxy. *Astrophys. J.* **2012**, *758*, 124.
21. Howley, K.M.; Guhathakurta, P.; van der Marel, R.; Geha, M.; Kalirai, J.; Yniguez, B.; Kirby, E.; Cuillandre, J.C.; Gilbert, K. Internal Stellar Kinematics of M32 from the SPLASH Survey: Dark Halo Constraints. *Astrophys. J.* **2013**, *765*, 65.
22. Dorman, C.E.; Guhathakurta, P.; Seth, A.C.; Weisz, D.R.; Bell, E.F.; Dalcanton, J.J.; Gilbert, K.M.; Hamren, K.M.; Lewis, A.R.; Skillman, E.D.; et al. A Clear Age-Velocity Dispersion Correlation in Andromeda's Stellar Disk. *Astrophys. J.* **2015**, *803*, 24.
23. McConnachie, A.W.; Huxor, A.; Martin, N.F.; Irwin, M.J.; Chapman, S.C.; Fahlman, G.; Ferguson, A.M.N.; Ibata, R.A.; Lewis, G.F.; Richer, H.; et al. A Trio of New Local Group Galaxies with Extreme Properties. *Astrophys. J.* **2008**, *688*, 1009–1020.
24. Dorman, C.E.; Widrow, L.M.; Guhathakurta, P.; Seth, A.C.; Foreman-Mackey, D.; Bell, E.F.; Dalcanton, J.J.; Gilbert, K.M.; Skillman, E.D.; Williams, B.F. A New Approach to Detailed Structural Decomposition from the SPLASH and PHAT Surveys: Kicked-up Disk Stars in the Andromeda Galaxy? *Astrophys. J.* **2013**, *779*, 103.
25. Gilbert, K.M.; Fardal, M.; Kalirai, J.S.; Guhathakurta, P.; Geha, M.C.; Isler, J.; Majewski, S.R.; Ostheimer, J.C.; Patterson, R.J.; Reitzel, D.B.; et al. Stellar Kinematics in the Complicated Inner Spheroid of M31: Discovery of Substructure along the Southeastern Minor Axis and Its Relationship to the Giant Southern Stream. *Astrophys. J.* **2007**, *668*, 245–267.
26. Gilbert, K.M.; Guhathakurta, P.; Kollipara, P.; Beaton, R.L.; Geha, M.C.; Kalirai, J.S.; Kirby, E.N.; Majewski, S.R.; Patterson, R.J. The Splash Survey: A Spectroscopic Portrait of Andromeda's Giant Southern Stream. *Astrophys. J.* **2009**, *705*, 1275–1297.
27. Gilbert, K.M.; Guhathakurta, P.; Beaton, R.L.; Bullock, J.; Geha, M.C.; Kalirai, J.S.; Kirby, E.N.; Majewski, S.R.; Ostheimer, J.C.; Patterson, R.J.; et al. Global Properties of M31's Stellar Halo from the SPLASH Survey. I. Surface Brightness Profile. *Astrophys. J.* **2012**, *760*, 76.
28. Williams, B.F.; Dalcanton, J.J.; Bell, E.F.; Gilbert, K.M.; Guhathakurta, P.; Lauer, T.R.; Seth, A.C.; Kalirai, J.S.; Rosenfield, P.; Girardi, L. The Panchromatic Hubble Andromeda Treasury. II. Tracing the Inner M31 Halo with Blue Horizontal Branch Stars. *Astrophys. J.* **2012**, *759*, 46.
29. Williams, B.F.; Dalcanton, J.J.; Bell, E.F.; Gilbert, K.M.; Guhathakurta, P.; Dorman, C.; Lauer, T.R.; Seth, A.C.; Kalirai, J.S.; Rosenfield, P.; et al. Tracing the Metal-poor M31 Stellar Halo with Blue Horizontal Branch Stars. *Astrophys. J.* **2015**, *802*, 49.
30. Seigar, M.S.; Barth, A.J.; Bullock, J.S. A revised Λ CDM mass model for the Andromeda Galaxy. *Mon. Not. R. Astron. Soc.* **2008**, *389*, 1911–1923.
31. Vargas, L.C.; Geha, M.C.; Tollerud, E.J. The Distribution of Alpha Elements in Andromeda Dwarf Galaxies. *Astrophys. J.* **2014**, *790*, 73.
32. Vargas, L.C.; Gilbert, K.M.; Geha, M.; Tollerud, E.J.; Kirby, E.N.; Guhathakurta, P. [α/Fe] Abundances of Four Outer M31 Halo Stars. *Astrophys. J. Lett.* **2014**, *797*, L2.

33. Kirby, E.N.; Cohen, J.G.; Guhathakurta, P.; Cheng, L.; Bullock, J.S.; Gallazzi, A. The Universal Stellar Mass-Stellar Metallicity Relation for Dwarf Galaxies. *Astrophys. J.* **2013**, *779*, 102.
34. Gilmore, G.; Wyse, R.F.G. Element Ratios and the Formation of the Stellar Halo. *Astron. J.* **1998**, *116*, 748–753.
35. Gilbert, K.M.; Font, A.S.; Johnston, K.V.; Guhathakurta, P. The Dominance of Metal-rich Streams in Stellar Halos: A Comparison Between Substructure in M31 and ΛCDM Models. *Astrophys. J.* **2009**, *701*, 776–786.
36. Gilbert, K.M.; Kalirai, J.S.; Guhathakurta, P.; Beaton, R.L.; Geha, M.C.; Kirby, E.N.; Majewski, S.R.; Patterson, R.J.; Tollerud, E.J.; Bullock, J.S.; et al. Global Properties of M31's Stellar Halo from the SPLASH Survey. II. Metallicity Profile. *Astrophys. J.* **2014**, *796*, 76.
37. Veljanoski, J.; Mackey, A.D.; Ferguson, A.M.N.; Huxor, A.P.; Côté, P.; Irwin, M.J.; Tanvir, N.R.; Peñarrubia, J.; Bernard, E.J.; Fardal, M.; et al. The outer halo globular cluster system of M31 - II. Kinematics. *Mon. Not. R. Astron. Soc.* **2014**, *442*, 2929–2950.
38. Wolf, J.; Martinez, G.D.; Bullock, J.S.; Kaplinghat, M.; Geha, M.; Muñoz, R.R.; Simon, J.D.; Avedo, F.F. Accurate masses for dispersion-supported galaxies. *Mon. Not. R. Astron. Soc.* **2010**, *406*, 1220–1237.
39. Watkins, L.L.; Evans, N.W.; An, J.H. The masses of the Milky Way and Andromeda galaxies. *Mon. Not. R. Astron. Soc.* **2010**, *406*, 264–278.
40. Guhathakurta, P.; Rich, R.M.; Reitzel, D.B.; Cooper, M.C.; Gilbert, K.M.; Majewski, S.R.; Ostheimer, J.C.; Geha, M.C.; Johnston, K.V.; Patterson, R.J. Dynamics and Stellar Content of the Giant Southern Stream in M31. I. Keck Spectroscopy of Red Giant Stars. *Astron. J.* **2006**, *131*, 2497–2513.
41. Kalirai, J.S.; Guhathakurta, P.; Gilbert, K.M.; Reitzel, D.B.; Majewski, S.R.; Rich, R.M.; Cooper, M.C. Kinematics and Metallicity of M31 Red Giants: The Giant Southern Stream and Discovery of a Second Cold Component at R = 20 kpc. *Astrophys. J.* **2006**, *641*, 268–280.
42. Fardal, M.A.; Guhathakurta, P.; Babul, A.; McConnachie, A.W. Investigating the Andromeda stream—III. A young shell system in M31. *Mon. Not. R. Astron. Soc.* **2007**, *380*, 15–32.
43. Fardal, M.A.; Guhathakurta, P.; Gilbert, K.M.; Tollerud, E.J.; Kalirai, J.S.; Tanaka, M.; Beaton, R.; Chiba, M.; Komiyama, Y.; Iye, M. A spectroscopic survey of Andromeda's Western Shelf. *Mon. Not. R. Astron. Soc.* **2012**, *423*, 3134–3147.
44. Fardal, M.A.; Weinberg, M.D.; Babul, A.; Irwin, M.J.; Guhathakurta, P.; Gilbert, K.M.; Ferguson, A.M.N.; Ibata, R.A.; Lewis, G.F.; Tanvir, N.R.; et al. Inferring the Andromeda Galaxy's mass from its giant southern stream with Bayesian simulation sampling. *Mon. Not. R. Astron. Soc.* **2013**, *434*, 2779–2802.
45. Irwin, M.J.; Ferguson, A.M.N.; Ibata, R.A.; Lewis, G.F.; Tanvir, N.R. A Minor-Axis Surface Brightness Profile for M31. *Astrophys. J. Lett.* **2005**, *628*, L105–L108, [arXiv:astro-ph/0505077].
46. Dorman, C.E.; Guhathakurta, P.; Fardal, M.A.; Lang, D.; Geha, M.C.; Howley, K.M.; Kalirai, J.S.; Bullock, J.S.; Cuillandre, J.C.; Dalcanton, J.J.; et al. The SPLASH Survey: Kinematics of Andromeda's Inner Spheroid. *Astrophys. J.* **2012**, *752*, 147.
47. Purcell, C.W.; Bullock, J.S.; Kazantzidis, S. Heated disc stars in the stellar halo. *Mon. Not. R. Astron. Soc.* **2010**, *404*, 1711–1718.
48. McCarthy, I.G.; Font, A.S.; Crain, R.A.; Deason, A.J.; Schaye, J.; Theuns, T. Global structure and kinematics of stellar haloes in cosmological hydrodynamic simulations. *Mon. Not. R. Astron. Soc.* **2012**, *420*, 2245–2262.
49. Tissera, P.B.; Scannapieco, C.; Beers, T.C.; Carollo, D. Stellar haloes of simulated Milky-Way-like galaxies: Chemical and kinematic properties. *Mon. Not. R. Astron. Soc.* **2013**, *432*, 3391–3400.